RESEARCH ARTICLE | APRIL 08 2025

Optimal multipole center for subwavelength acoustic scatterers

N. Ustimenko ; C. Rockstuhl ; A. V. Kildishev

Appl. Phys. Lett. 126, 142201 (2025)
https://doi.org/10.1063/5.0257760

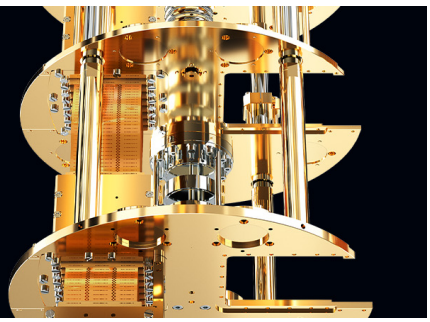

Applied Physics Letters ARTICLE pubs.aip.org/aip/apl

Optimal multipole center for subwavelength acoustic scatterers

Cite as: Appl. Phys. Lett. **126**, 142201 (2025); doi: 10.1063/5.0257760
Submitted: 12 January 2025 · Accepted: 24 March 2025 ·
Published Online: 8 April 2025

N. Ustimenko,[1] C. Rockstuhl,[1,2] and A. V. Kildishev[3,a)]

AFFILIATIONS

[1]Institute of Theoretical Solid State Physics, Karlsruhe Institute of Technology, Kaiserstrasse 12, Karlsruhe D-76131, Germany
[2]Institute of Nanotechnology, Karlsruhe Institute of Technology, Kaiserstrasse 12, Karlsruhe D-76131, Germany
[3]Elmore Family School of Electrical and Computer Engineering and Birck Nanotechnology Center, Purdue University, 1205 W State St, West Lafayette, Indiana 47907, USA

[a)]Author to whom correspondence should be addressed: kildishev@purdue.edu

ABSTRACT

The multipole expansion is a powerful framework for analyzing how subwavelength-size objects scatter waves in optics or acoustics. The calculation of multipole moments traditionally uses the scatterer's center of mass as the reference point. The theoretical foundation of this heuristic convention remains an open question. Here, we challenge this convention by demonstrating that a different, optimal multipole center (OMC) can yield superior results. The optimal center is crucial—it allows us to accurately express the scattering response while retaining a minimum number of multipole moments. Our analytical technique for finding the optimal multipole centers of individual scatterers, both in isolation and within finite arrays, is validated through numerical simulations. Our findings reveal that such an optimized positioning significantly reduces quadrupole contributions, enabling more accurate monopole–dipole approximations in acoustic calculations. Our approach also improves the computational efficiency of the T-matrix method, offering practical benefits for metamaterial design and analysis.

The efficient modeling of sound scattering by finite heterogeneous arrays of compact objects (scatterers) varying in shape and material properties represents a fundamental challenge in acoustics. This problem has gained renewed attention with the advent of modern high-performance computing, which has enabled the practical implementation of transition matrix (T-matrix) schemes.[1–7] Contemporary T-matrix frameworks can accurately capture complex interactions among arrayed scatterers, even when the individual scatterers exhibit structural and material diversity. This capability becomes particularly critical in the emerging field of inverse-designed metamaterials[8–17] and their physics-based optimization algorithms using T-matrix solvers.[18–22] The classical[23–26] and more recent studies[28–36] on multipole expansion, a versatile method for modeling scattering by subwavelength scatterers in optics and acoustics, form the basis of these approaches.

In the T-matrix method, the incident and scattered fields for any compact scatterer are expressed as a truncated multipole expansion. The selection of the spatial coordinate relative to which these fields are expanded is critical to the accuracy of the method. Frequently, the multipoles are positioned at the scatterer's center of mass.[37] However, the multipole moments induced in a scatterer by incident fields depend on the chosen expansion center, and generally, no unique choice exists.[37,38] An arbitrary coordinate center can be selected as the expansion center, but it requires retaining an increasing number of multipoles in the expansion to express the scattering response accurately. Computationally, this quickly becomes extremely demanding, if not impossible. Therefore, identifying an optimal center is critical to minimize the number of multipole terms retained in the expansion.

Our study addresses this challenge in acoustics by seeking to minimize the number of multipoles retained in the expansion when describing the acoustic scattering response from either scatterers or finite arrays thereof. Through both analytical and numerical approaches, we examine the scattering of acoustic pressure waves by subwavelength scatterers to determine the location of the optimal multipole center (OMC). We demonstrate that selecting this optimal center minimizes the quadrupole contribution, creating ideal conditions for applying the monopole–dipole approximation (MDA) in acoustics widely used in the literature.[39–43] This approach can be applied to both isolated scatterers and compact arrays where simple multipole sources interact at short distances.

We begin with a mathematical formulation of our problem. The scattered pressure $p_{\mathrm{sca}}(k;\mathbf{r})$ of an acoustic scatterer can be expressed as a truncated expansion in scalar spherical waves (multipoles) weighted by multipole moments,[44]

$$p_{\mathrm{sca}}(k;\mathbf{r}) = \sum_{\ell=0}^{\ell_{\max}} \sum_{m=-\ell}^{\ell} p_{\ell,m}(k;\mathbf{d})\psi^{(3)}_{\ell,m}(k;\mathbf{r}-\mathbf{d}), \tag{1}$$

where ℓ and m are the degree and order of the singular multipole $\psi^{(3)}_{\ell,m}(k;\mathbf{r}-\mathbf{d})$ (see Sec. S1 A in the supplementary material for its definition). $\mathbf{r} \neq \mathbf{d}$ and $k = \omega/c_0$ is the wavenumber in the surrounding medium. $\mathbf{d}$ is an offset of the multipole center relative to the scatterer's center of mass defined as $\mathbf{r}_{\mathrm{CM}} = \mathbf{0}$ [point O in Fig. 1(a)]. For Eq. (1) to be valid, the coordinate $\mathbf{r}$ must belong to the space region outside a sphere circumscribing the scatterer.[45] We aim to choose the optimal $\mathbf{d}_{\mathrm{opt}}$ that simultaneously provides the best precision in calculating physical quantities and the lowest maximal multipole degree $\ell_{\max}$ in the expansion. In this work, we assume that the offset $\mathbf{d}$ is subwavelength, that is, $k|\mathbf{d}| \ll 1$.

To determine $\mathbf{d}_{\mathrm{opt}}$, we need to know the dependence of the multipole moments on $\mathbf{d}$. Using the translation coefficients of spherical waves $\alpha^{(1)}_{\ell m \ell' m'}(k;\mathbf{d})$ (sec. S1 C in the supplementary material),[46] we link the multipole moments obtained for an expansion center shifted to $\mathbf{d}$ to the multipole moments obtained at the center of mass, i.e., at $\mathbf{d} = \mathbf{0}$ (see Sec. S1 D in the supplementary material),

$$p_{\ell,m}(k;\mathbf{d}) = \sum_{\ell'=0}^{\ell_{\max}} \sum_{m'=-\ell'}^{\ell'} \alpha^{(1)}_{\ell m \ell' m'}(k;\mathbf{d}) p_{\ell',m'}(k;\mathbf{0}), \tag{2}$$

where $p_{\ell',m'}(k;\mathbf{0})$ can be computed using, e.g., the acoustic T-matrix of the scatterer[47,48] (see Sec. S6 in the supplementary material) or upon post-processing simulations from a full-wave solver (see, e.g., Appendix B in Refs. 49 and 50). Equation (2) is of significant practical importance—it shows that to obtain the entire dependence of the multipole moments on $\mathbf{d}$, we *can calculate the multipole moments only once*, if the chosen $\ell_{\max}$ is sufficient.

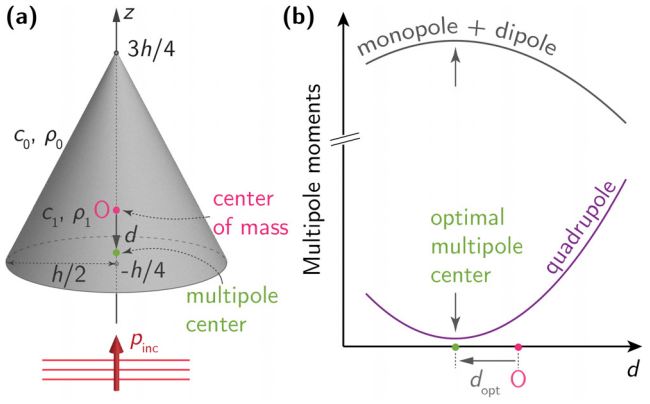

FIG. 1. Sketch of the considered problem. (a) A cone of height h under insonification of an acoustic plane wave propagating along the z-axis. The center of the multipole expansion (green point) is offset from the center of mass (pink point O, $z = 0$) by a distance d. (b) Squared amplitudes of first three multipole moments of the cone vs d at a fixed frequency. The quadrupole moment exhibits a minimum, whereas the sum of the monopole and dipole moments has a maximum, manifesting the optimal multipole center's position $z = d_{\mathrm{opt}}$.

Furthermore, we verify our semi-analytical approach in two examples. As a first example, we find the OMC for a cone-shaped scatterer with cylindrical symmetry along the z-axis [see Fig. 1(a)]. The symmetry is conserved for a plane wave excitation along the z-axis, and only the zonal multipoles (with $m = 0$) are excited. Moreover, the offset along the z-axis $\mathbf{d} = d\hat{\mathbf{z}}$ affects only the zonal multipole content of the scatterer because the shifted system remains axisymmetric. Furthermore, we consider a spectral range where the first three multipoles sufficiently approximate the scattering for all d we examine, i.e., $\ell_{\max} = 2$ can be held. In this case, the scattering cross section of the cone is $\sigma_{\mathrm{tot}}(k) = k^{-2}\sum_{\ell=0}^{\ell_{\max}} |p_{\ell,0}(k;\mathbf{d})|^2$. Here, we consider the offsets d that are sufficiently small to make $\sigma_{\mathrm{tot}}(k)$ almost independent of $\mathbf{d}$, while its MDA $\sigma_{\mathrm{md}}(k;\mathbf{d}) = k^{-2}\sum_{\ell=0}^{1} |p_{\ell,0}(k;\mathbf{d})|^2$ still depends on $\mathbf{d}$. Therefore, we define $\mathbf{d}_{\mathrm{opt}}$ as $\min_{\mathbf{d}} |p_{2,0}(k;\mathbf{d})|^2$ for a given k to reduce error $|\sigma_{\mathrm{md}}(k;\mathbf{d}) - \sigma_{\mathrm{tot}}(k)|$. We then compute $\mathbf{d}_{\mathrm{opt}}$ from equation $\nabla_{\mathbf{d}} |p_{2,0}(k;\mathbf{d})|^2 = 0$.

Although standard numerical methods[51] can be used to find $\mathbf{d}_{\mathrm{opt}}$, we solve this problem analytically. We start by adapting Eq. (2) to the considered case and write the off-origin quadrupole moment as a function of a normalized offset (kd). For all zonal multipole coefficients, we make substitutions $p_2(kd) \equiv p_{2,0}(k;d\hat{\mathbf{z}})$ and $p_\ell \equiv p_{\ell,0}(k;\mathbf{0})$ for brevity and then arrive at the following compact equation:

$$p_2(kd) = p_2 + \mathbf{A}_2(kd)\cdot\mathbf{p}, \tag{3}$$

with $\mathbf{p} = [p_0, p_1, p_2]^{\mathrm{T}}$, $\mathbf{A}_2(kd) = [\alpha_0(kd), \alpha_1(kd), \alpha_2(kd)]^{\mathrm{T}}$, and $\alpha_{\ell'}(kd) \equiv \alpha^{(1)}_{20\ell'0}(k;d\hat{\mathbf{z}}) - \delta_{2,\ell'}$. The long-wavelength approximation (LWA) $kd \ll 1$ of the spherical Bessel functions (see Sec. S1 B in the supplementary material) gives an approximate separation vector $\tilde{\mathbf{A}}_2(kd) = [\tilde{\alpha}_0(kd), \tilde{\alpha}_1(kd), \tilde{\alpha}_2(kd)]^{\mathrm{T}}$,

$$\tilde{\mathbf{A}}_2(kd) = \left[\frac{1}{3\sqrt{5}}(kd)^2, -\frac{2}{\sqrt{15}}(kd), -\frac{11}{42}(kd)^2\right]^{\mathrm{T}}, \tag{4}$$

where the tilde is used to distinguish the accurate values of translation coefficients $\alpha_{\ell'}$ from their LWA $\tilde{\alpha}_{\ell'}$. After substituting Eq. (4) into Eq. (3), we arrive at a quadratic approximation of $|p_2(kd)|^2$,

$$|\tilde{p}_2(kd)|^2 = f_{0,k} + f_{1,k}(kd) + f_{2,k}(kd)^2, \tag{5}$$

where $f_{0,k} = |p_2|^2$, $f_{1,k} = -\frac{4}{\sqrt{15}}\Re[p_1^* p_2]$, and $f_{2,k} = \frac{4}{15}|p_1|^2 - \frac{11}{21}|p_2|^2 + \frac{2}{3\sqrt{5}}\Re[p_0^* p_2]$ with a real k (for a complex k, we refer to Sec. S2 C in the supplementary material) and $p_\ell = p_\ell(k)$, calculated for $d = 0$. The accuracy of Eqs. (3) and (5) in the considered spectral range is confirmed in Sec. S2 A in the supplementary material. Similar interpolations can be derived for the coefficients $p_0(kd)$ and $p_1(kd)$ (see Sec. S2 B in the supplementary material) as well as for high-degree terms. The main outcome of (5) is an analytical formula for the optimal offset being a solution to the equation $\partial_{(kd)}|\tilde{p}_2(kd)|^2 = 0$ (k is fixed) that provides $d_{\mathrm{opt}} = -f_{1,k}/(2kf_{2,k})$ or

$$d_{\mathrm{opt}} = \frac{\sqrt{3}}{k}\frac{\Re[p_1^* p_2]}{\frac{2}{\sqrt{5}}|p_1|^2 - \frac{11\sqrt{5}}{14}|p_2|^2 + \Re[p_0^* p_2]}, \tag{6}$$

where the sign of second derivative $f_{2,k} > 0$ and $k \neq 0$ has been implied. Thus, once the multipole moments at $d = 0$ are known, the OMC's position is directly given by Eq. (6). Moreover, Eq. (6) can be used even if the initial multipole center is at an arbitrary point $d = d_0$. Then, a translation $(d_{\text{opt}} + d_0)$ gives the OMC.

To increase the accuracy, one can extend expansion (5) up to the next even power of (kd),

$$|\breve{p}_2(kd)|^2 = \sum_{n=0}^{4} f_{n,k}(kd)^n, \tag{7}$$

where $f_{3,k}$ and $f_{4,k}$ are given in Sec. S2 C in the supplementary material. In this case, an optimal offset is calculated as a pure real solution to the cubic equation $\partial_{(kd)}|\breve{p}_2(kd)|^2 = 0$ being

$$f_{1,k} + 2f_{2,k}(kd) + 3f_{3,k}(kd)^2 + 4f_{4,k}(kd)^3 = 0. \tag{8}$$

To validate the analytical results, we perform a numerical simulation of the scattering of a plane wave by a cone of height $h = 1$ cm and radius of $h/2$. The cone is made of a material with the speed of sound c_1 and mass density ρ_1. It is placed in a medium with $c_0/c_1 = \sqrt{21}$ and $\rho_0/\rho_1 = 1/7$ [see Fig. 1(a)]. We use our in-house T-matrix-based code *acoustotreams*,[52] which is an adaptation of the electromagnetic scattering code *treams* for acoustic scattering.[53] The acoustic T-matrix of the cone was calculated for $d = 0$ in a spectral range between 5 and 25.5 kHz with a step of 0.1 kHz using the finite-element method (Pressure Acoustics interface in COMSOL Multiphysics, v. 6.2).[54] The acoustic T-matrix was then exported to *acoustotreams* to calculate the offset multipole moments (2) with $\ell_{\max} = 5$ (full-wave model).

Figure 2 presents the results of the full-wave numerical simulations, which are the cone scattering efficiency in (a), the normalized quadrupole moment map in (b) with numerical values of d_{opt} shown by green markers, and the relative error for the MDA of the scattering cross section in (c) calculated for the multipole center placed at the center of mass and OMC (numerical values). Figure 2(b) also compares the numerical values of d_{opt} to the analytical values in the quadratic (6) and quartic (8) approximations. Multiple observations can be made.

First, the OMC converges to $d_{\text{opt}} = -0.075$ cm in a subwavelength regime $\omega h/c_0 \lesssim 1$ [see Fig. 2(b)]. Thus, the OMC is located below the center of mass, similar to the magnetic multipole center of electromagnetic scatterers.[55] The OMCs predicted by all three models coincide for $\omega h/c_0 < 2.75$ except at the monopole resonance $\omega_{\text{I}} h/c_0 = 1.68$. At this frequency, the quartic approximation $|\breve{p}_2|^2$ fails near the actual minimum of $|p_2|^2$ taking nonphysical negative values. Therefore, the sextic approximation should be used. We do not show it here for brevity, but it can be found in Sec. S2 C 4 in the supplementary material. For optical scatterers, we have already demonstrated that the optimal multipole center differs from the scatterer's center of mass and is, in fact, dispersive.[55] In contrast, at dipole resonance $\omega_{\text{II}} h/c_0 = 2.4$, all models predict the same OMC with a significant suppression of the error [see the inset in Fig. 2(c)]. In Fig. 2(b), we also see that the negative OMC turns into a large positive OMC around $\omega_{\text{III}} h/c_0 \simeq 2.75$ (the gray region in Fig. 2), and the second derivatives of (5) and (7) become negative (see Sec. S3 in the supplementary material). In this case, the monopole contribution to the scattering is suppressed, while the quadrupole becomes substantial. Figure 2(c) also confirms that neglecting the quadrupole around

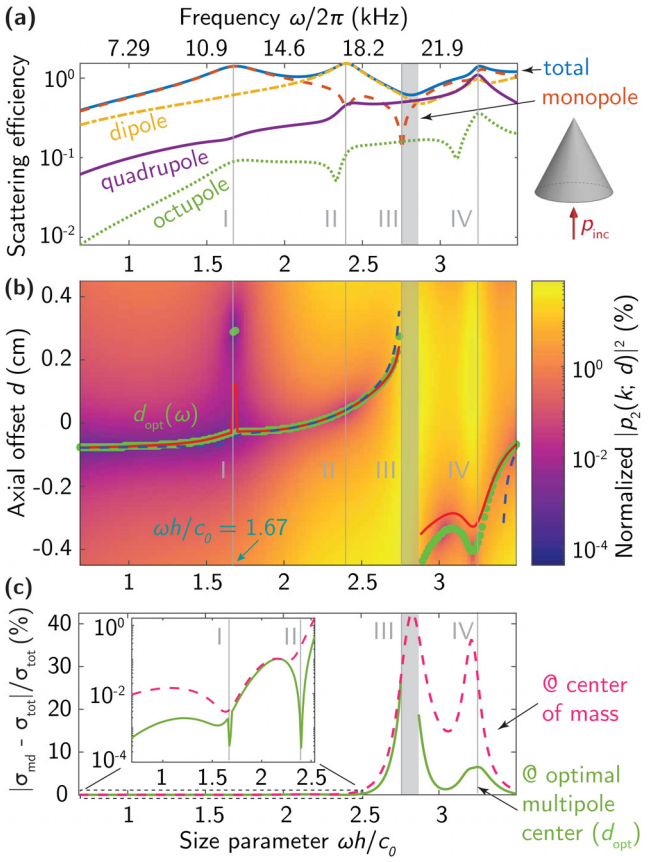

FIG. 2. (a) Scattering efficiency $\sigma_{\text{tot}}(k)/(0.25\pi h^2)$ of the cone, shown in the inset, with its multipole decomposition for the multipole center at $d = 0$. (b) Normalized zonal quadrupole moment of the cone $|p_2(k;d)|^2/\sum_{\ell\neq 2}|p_\ell(k;d)|^2$ for $\ell_{\max} = 5$. The green dots show the values of $d_{\text{opt}} = \min_d |p_2(k;d)|^2$, obtained directly from the full-wave numerical simulations. The dashed blue and solid red lines show d_{opt} calculated with the quadratic [Eq. (6)] and quartic [Eq. (8)] approximations of $|p_2(k;d)|^2$, respectively. (c) Error of the scattering cross section for $\ell_{\max} = 1$ relative to that for $\ell_{\max} = 5$ at $d = 0$ (pink dashed) and $d = d_{\text{opt}}$, calculated in the full-wave model (green solid). Inset: the same but on a logarithmic scale for $\omega h/c_0 \leq 2.5$.

$\omega \simeq \omega_{\text{III}}$ leads to an error larger than 40%. Hence, the OMC should be redefined as a minimum of a higher-degree multipole moment. Surprisingly, at the quadrupole resonance $\omega_{\text{IV}} h/c_0 = 3.24$, the quadrupole moment can still be neglected with an error of 10% since the monopole also exhibits a resonant-like response. Thus, a center for the multipole expansion of the fields placed at the optimal point provides the best conditions for the MDA. The error in the scattering cross section is consistently smaller when the OMC is chosen for the expansion compared to when the center of mass is chosen [see Fig. 2(c)]. At the same time, one can use Eq. (6) to predict the positions of the OMC for $\omega h/c_0 \leq 2.75$ when $f_{2,k} > 0$. For higher frequencies, Eq. (8) or the higher approximations should be employed [see Fig. 2(b)].

In a further analysis, we demonstrate that the OMC can be found not only for individual scatterers but also for finite arrangements thereof. The framework of the T-matrix method can be efficiently applied to acoustic multiple scattering problems,[56–58] where one needs

to distinguish a formulation in a local and global description of the scattered fields of arrangements.[59] In the local description (LD), the fields are expanded at the N local positions of all N scatterers, $\mathbf{r}_i$ with $i = 1..N$. The multiple scattering equation is solved to obtain the self-consistent multipole moments that account for the interactions of the scatterers with the incident field and with each other [see, e.g., Eq. (17) in Ref. 53]. In the LD, the multipole moments are calculated when the multipole centers coincide with the centers of mass of scatterers located at $\mathbf{r}_i$. In the global description (GD), the fields are expanded from all particles using a global expansion center at a single point $\mathbf{d}$. In this regard, the global multipole moments depend on $\mathbf{d}$ and the local multipole moments as

$$p^{(\mathrm{global})}_{\ell,m}(k;\mathbf{d}) = \sum_{\ell'=0}^{\ell_{\max}} \sum_{m'=-\ell'}^{\ell'} \sum_{i=1}^{N} \alpha^{(1)}_{\ell m \ell' m'}(k;\mathbf{d}-\mathbf{r}_i) p^{(\mathrm{local})}_{\ell',m'}(k;\mathbf{r}_i). \quad (9)$$

Equation (9) is similar to Eq. (2) for the single-particle case, but it includes a sum over the scatterers. The other feature is more inconspicuous. The maximal multipole degree in the GD $L_{\max}$ can be larger than in the LD $\ell_{\max}$. Thus, a transition from the LD to the GD is reasonable when the size of an arrangement T-matrix in the GD, $(L_{\max}+1)^2$, is smaller than the size of an arrangement T-matrix in the LD, $N(\ell_{\max}+1)^2$.

As an example, we consider a trimer of spherical particles shown in Fig. 3(a). The spheres of radius $R = 0.5$ cm are placed at the nodes of an equilateral triangle of side $a = 3R$. The material parameters (mass density and speed of sound) of the scatterer material and the background are the same as before. Hereafter, we can use the same formalism as before but in a multiple scattering scenario to find the minima of the quadrupole moment in the GD $\sum_{m=-2}^{2} |p^{(\mathrm{global})}_{2,m}(k;\mathbf{d})|^2$. An interaction between the spheres can induce the multipoles with $m \neq 0$. However, their contribution is smaller than that of zonal multipoles. Therefore, we can apply Eqs. (6) and (8) to predict d_{opt}. We assume the range of frequencies 1–11 kHz where $\ell_{\max} = 1$ and $L_{\max} = 2$ are sufficient. If we manage to find the OMC where even $L_{\max} = 1$ provides good accuracy, then we will decrease the size of the trimer T-matrix from 12 to 4, although one has to track $d_{\mathrm{opt}}(\omega)$.

Figure 3 presents the same content as Fig. 2 but for the trimer. The main difference lies in the behavior of d_{opt}. In the static case, the system is symmetric concerning the rotations by $\pi/3$ and $2\pi/3$ in the xz plane; hence, $d_{\mathrm{opt}} \to 0$ when $\omega a'/c_0 \to 0$, i.e., the OMC coincides with the center of mass of the trimer [see Fig. 3(b)]. Here, $\omega a'/c_0$ is an effective trimer size parameter with $a' = a + 2R$. As $\omega a'/c_0$ increases, d_{opt} also increases. From $\omega a'/c_0 = 2.6$, the OMC remains at the same point $d_{\mathrm{opt}} \approx 0.35$ cm close to the center of the upper sphere and provides a better accuracy of the MDA [see Fig. 3(c)]. Both quadratic and quartic models predict d_{opt} for $\omega a'/c_0 \leq 2.6$ very well, although the quadratic model fails for $\omega a'/c_0 > 2.6$ due to the resonant response of the trimer [see Fig. 3(a)]. In Sec. S4 in the supplementary material, we also consider this trimer rotated by $\pi/2$ in the xz plane, for which $\mathbf{d}_{\mathrm{opt}}$ is traced as a trajectory, with the initial point at $\mathbf{d}_{\mathrm{opt}} = \mathbf{0}$, as the frequency increases.

In the end, we demonstrate that the OMC can improve the computational efficiency of the acoustic T-matrix method in multiple scattering problems. For that purpose, we consider a ring of N identical cones (the same as those previously considered) placed at a distance $D = 2.6$ cm between the nearest neighbors. The acoustic T-matrix of the individual cone is calculated at frequency $\omega h/c_0 = 2.5$ for the multipole expansion center placed at $d = 0$ with $\ell_{\max} = 2$, and at the OMC with $\ell_{\max} = 1$ [see Fig. 2(b)]. An additional modification of the OMCs due to the interaction between scatterers is neglected. Then, we vary N from 80 to 380, estimate the time we need to solve the multiple scattering problem, compute the ring scattering cross section for each N, average this time after 10 iterations, and normalize it by τ. Here, τ is the average time to solve a linear system with a 1000×1000 matrix and 1000×1 right-hand side using the *numpy.linalg.solve* function in Python 3.11.

Figure 4 illustrates the results, demonstrating that the OMC reduces computational time by a factor of six, as we reduce the size of

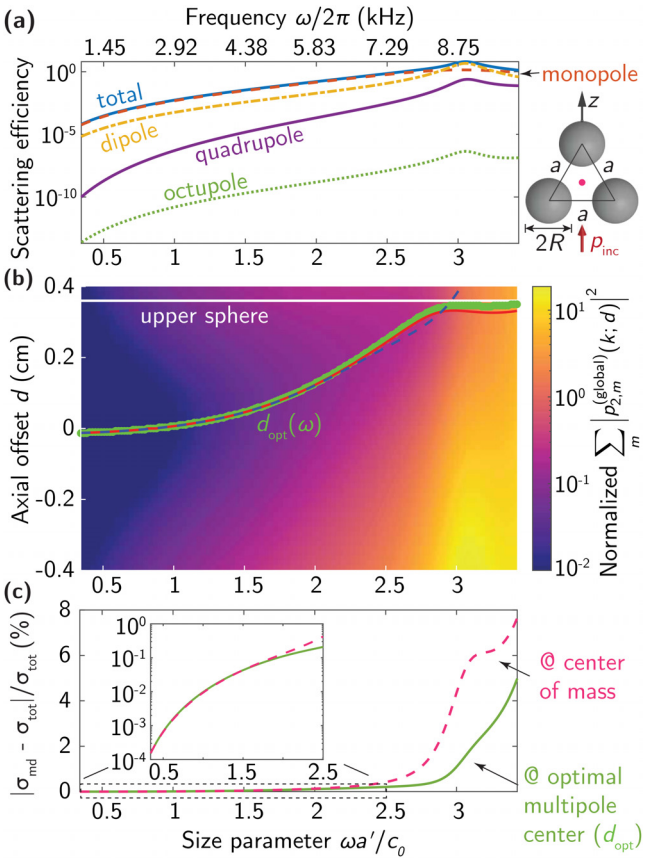

FIG. 3. The same as in Fig. 2 but for a trimer of spherical scatterers [see the inset of panel (a)] using the global description (9) of the trimer acoustic response. (a) The scattering efficiency is $\sigma_{\mathrm{tot}}(k)/(0.25\pi[a']^2)$ where $a' = a + 2R$. The pink dot indicates the center of mass. (b) Normalized global quadrupole moment of the trimer $\sum_m |p^{(\mathrm{global})}_{2,m}(k;d)|^2 / \sum_{\ell\neq 2,m} |p^{(\mathrm{global})}_{\ell,m}(k;d)|^2$ for $\ell_{\max} = 2$ and $L_{\max} = 4$. The green dots show the values of $d_{\mathrm{opt}} = \min_d \sum_m |p^{(\mathrm{global})}_{2,m}(k;d)|^2$, obtained directly from the full-wave numerical simulations. The dashed blue and solid red lines show d_{opt} calculated with the quadratic [Eq. (6)] and quartic [Eq. (8)] approximations of the zonal term $|p^{(\mathrm{global})}_{2,0}(k;d)|^2$, respectively. (c) Error of the scattering cross section for $L_{\max} = 1$ relative to that for $L_{\max} = 4$ at $d = 0$ (pink dashed) and $d = d_{\mathrm{opt}}$, calculated in the full-wave model (green solid). Inset: the same but on a logarithmic scale for $\omega a'/c_0 \leq 2.5$.

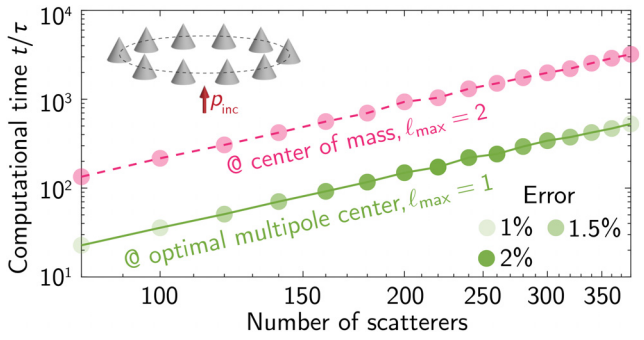

FIG. 4. Normalized computational time vs the number of cone-shaped scatterers arranged in a ring depicted in the inset. The expansion center for the single cone is placed at either its center of mass with $\ell_{max} = 2$ (pink dashed) or the OMC with $\ell_{max} = 1$ (green solid). The transparency of the markers indicates the corresponding error of the scattering cross section.

the isolated-cone T-matrix from 9 for $\ell_{max} = 2$ to 4 for $\ell_{max} = 1$, while the error in the calculation of the ring scattering cross section remains comparable. Moreover, using the MDA but placing the multipole center at the center of mass increases the average error from 1.42% to 4%. Thus, the OMC remarkably reduces the computational time within the T-matrix and multipole methods for simulating the acoustic response of discrete scatterers while maintaining a reasonable error.

As drawbacks of the OMC approach, we have to mention first that an offset d of the multipole expansion center effectively increases the radius of a sphere circumscribing the scatterer from R_c to $(R_c + d)$. Expansion (1) becomes then valid outside a larger circumscribing sphere,[45] which may lead to larger minimal spacings between the scatterers in their arrangements. Moreover, the OMC, as discussed here, has been found for a particular incidence of the external wave along the z-axis. As discussed in Ref. 55, a different illumination direction leads to different OMCs, making the OMC both frequency- and angular-dispersive (see Sec. S5 in the supplementary material).

In conclusion, we address the problem of determining the optimal point to place the multipole expansion center in acoustic scattering. We consider individual scatterers and multi-particle structures without reflection symmetry along the z-axis and trace the OMC position along the axis when the scatterers are insonified by a plane wave. Our comprehensive acoustic scattering model reveals that similar to electromagnetic scattering,[55] an optimal solution minimizes the multipole content to produce the most efficient descriptor while retaining only a few terms of the lowest degree. We showcase the advantages of using low-degree multipoles (monopole and dipole) at this OMC, demonstrating substantial computational efficiency gains achieved in T-matrix calculations. Our approach can be extended beyond the systems described within the monopole–dipole–quadrupole approximation to systems of arbitrary geometry that require optimizing their multipole descriptions up to arbitrary multipole degrees and orders.

See the supplementary material for the definition of scalar spherical waves (multipoles), the addition theorem and translation coefficients, the derivation of Eqs. (3)–(8), the analysis of the error of approximations (3), (4), and (7), the calculation of an optimal multipole center trajectory for the rotated trimer, the calculation of an optimal multipole center for the isolated cone as a function of the angle of incidence, and the details on the computation of the acoustic T-matrices of axisymmetric objects in COMSOL Multiphysics.

The authors acknowledge Markus Nyman for helping with the numerical simulations. N. U. and C. R. acknowledge support from the Deutsche Forschungsgemeinschaft (DFG, German Research Foundation) under Germany's Excellence Strategy via the Excellence Cluster 3D Matter Made to Order (EXC-2082/1, Grant No. 390761711) and from the Carl Zeiss Foundation via CZF-Focus@HEiKA.

AUTHOR DECLARATIONS

Conflict of Interest

The authors have no conflicts to disclose.

Author Contributions

N. Ustimenko: Methodology (equal); Software (lead); Visualization (lead); Writing – original draft (lead); Writing – review & editing (equal). **C. Rockstuhl:** Conceptualization (equal); Funding acquisition (lead); Writing – review & editing (equal). **A. V. Kildishev:** Conceptualization (equal); Methodology (equal); Supervision (lead); Writing – review & editing (equal).

DATA AVAILABILITY

The data that support the findings of this study are openly available in GitHub, Ref. 52.

REFERENCES

[1]L. E. Kinsler, A. R. Frey, A. B. Coppens, and J. V. Sanders, *Fundamentals of Acoustics*, 4th ed. (John Wiley & Sons Inc., Hoboken, NJ, 1999).
[2]R. Sainidou, N. Stefanou, I. E. Psarobas, and A. Modinos, Comput. Phys. Commun. **166**, 197 (2005).
[3]Z. Gong, W. Li, Y. Chai, Y. Zhao, and F. G. Mitri, Ocean Eng. **129**, 507 (2017).
[4]Z. Gong, P. L. Marston, and W. Li, Phys. Rev. E **99**, 063004 (2019).
[5]M. Ganesh and S. C. Hawkins, J. Acoust. Soc. Am. **151**, 1978 (2022).
[6]Y. Yang, Q. Gui, Y. Zhang, Y. Chai, and W. Li, Front. Phys. **11**, 1170811 (2023).
[7]Z. Li, P. Han, and G. Hu, J. Mech. Phys. Solids **189**, 105692 (2024).
[8]M. R. Haberman and M. D. Guild, Phys. Today **69**(6), 42 (2016).
[9]Z. Wang, Q. Zhang, K. Zhang, and G. Hu, Adv. Mater. **28**, 9857 (2016).
[10]K. Bertoldi, V. Vitelli, J. Christensen, and M. van Hecke, Nat. Rev. Mater. **2**, 1 (2017).
[11]C. F. Sieck, A. Alù, and M. R. Haberman, Phys. Rev. B **96**, 104303 (2017).
[12]D. Colton and R. Kress, *Inverse Acoustic and Electromagnetic Scattering Theory* (Springer International Publishing, Cham, Switzerland, 2019).
[13]H. Ronellenfitsch, N. Stoop, J. Yu, A. Forrow, and J. Dunkel, Phys. Rev. Mater. **3**, 095201 (2019).
[14]A. Krishna, S. R. Craig, C. Shi, and V. R. Joseph, Appl. Phys. Lett. **121**, 071701 (2022).
[15]H. Long, Y. Zhu, Y. Gu, Y. Cheng, and X. Liu, Phys. Rev. Appl. **18**, 044032 (2022).
[16]Z. Li, Y. Sun, G. Wu, and M. Tao, Appl. Acoust. **204**, 109247 (2023).
[17]B. Fang, R. Zhang, T. Chen, W. Wang, J. Zhu, and W. Cheng, J. Build. Eng. **86**, 108898 (2024).
[18]A. Zhan, T. K. Fryett, S. Colburn, and A. Majumdar, Appl. Opt. **57**, 1437 (2018).
[19]M. V. Zhelyeznyakov, A. Zhan, and A. Majumdar, OSA Continuum **3**, 89 (2020).

[20]N. Ustimenko, K. V. Baryshnikova, R. Melnikov, D. Kornovan, V. Ulyantsev, B. N. Chichkov, and A. B. Evlyukhin, J. Opt. Soc. Am. B **38**, 3009 (2021).
[21]S. Gladyshev, T. D. Karamanos, L. Kuhn, D. Beutel, T. Weiss, C. Rockstuhl, and A. Bogdanov, Nanophotonics **12**, 3767 (2023).
[22]P. Garg, J. D. Fischbach, A. G. Lamprianidis, X. Wang, M. S. Mirmoosa, V. S. Asadchy, C. Rockstuhl, and T. J. Sturges, arXiv.2409.04551 (2024).
[23]A. Clebsch, J. Reine Angew. Math. **1863**, 195.
[24]G. Mie, Ann. Phys. **330**, 377 (1908).
[25]L. Lorenz, Eur. Phys. J. H **44**, 77 (2019).
[26]Reference 25 above has been translated from the original Danish text Ref. 27 by Jeppe Revall Frisvad, DTU, and Helge Kragh, U. of Copenhagen, Denmark.
[27]L. Lorenz, Det kongelige danske Videnskabernes Selskabs Skrifter **6**, 1 (1890).
[28]S. Mühlig, C. Menzel, C. Rockstuhl, and F. Lederer, Metamaterials **5**, 64 (2011).
[29]I. Fernandez-Corbaton, S. Nanz, R. Alaee, and C. Rockstuhl, Opt. Express **23**, 33044 (2015).
[30]A. B. Evlyukhin, T. Fischer, C. Reinhardt, and B. N. Chichkov, Phys. Rev. B **94**, 205434 (2016).
[31]D. Smirnova and Y. S. Kivshar, Optica **3**, 1241 (2016).
[32]X. Zhu, B. Liang, W. Kan, Y. Peng, and J. Cheng, Phys. Rev. Appl. **5**, 054015 (2016).
[33]R. Alaee, C. Rockstuhl, and I. Fernandez-Corbaton, Opt. Commun. **407**, 17 (2018).
[34]R. Alaee, C. Rockstuhl, and I. Fernandez-Corbaton, Adv. Opt. Mater. **7**, 1800783 (2019).
[35]D. A. Kovacevich and B.-I. Popa, Phys. Rev. B **104**, 134304 (2021).
[36]M. Riccardi, A. Kiselev, K. Achouri, and O. J. F. Martin, Phys. Rev. B **106**, 115428 (2022).
[37]A. B. Evlyukhin, C. Reinhardt, and B. N. Chichkov, Phys. Rev. B **84**, 235429 (2011).
[38]A. B. Evlyukhin, C. Reinhardt, E. Evlyukhin, and B. N. Chichkov, J. Opt. Soc. Am. B **30**, 2589 (2013).
[39]G. T. Silva, J. Acoust. Soc. Am. **136**, 2405 (2014).
[40]I. D. Toftul, K. Y. Bliokh, M. I. Petrov, and F. Nori, Phys. Rev. Lett. **123**, 183901 (2019).
[41]L. Wei and F. J. Rodríguez-Fortuño, New J. Phys. **22**, 083016 (2020).
[42]Y. Long, H. Ge, D. Zhang, X. Xu, J. Ren, M.-H. Lu, M. Bao, H. Chen, and Y.-F. Chen, Natl. Sci. Rev. **7**, 1024 (2020).
[43]M. Smagin, I. Toftul, K. Y. Bliokh, and M. Petrov, Phys. Rev. Appl. **22**, 064041 (2024).
[44]D. T. Blackstock, *Fundamentals of Physical Acoustics* (Wiley, Hoboken, NJ, 2000).
[45]B. Auguié, W. R. C. Somerville, S. Roache, and E. C. Le Ru, J. Opt. **18**, 075007 (2016).
[46]P. A. Martin, *Multiple Scattering: Interaction of Time-Harmonic Waves With N Obstacles* (Cambridge University Press, Cambridge, England, UK, 2006).
[47]P. C. Waterman, J. Acoust. Soc. Am. **45**, 1417 (1969).
[48]P. C. Waterman, J. Acoust. Soc. Am. **125**, 42 (2009).
[49]M. Tsimokha, V. Igoshin, A. Nikitina, I. Toftul, K. Frizyuk, and M. Petrov, Phys. Rev. B **105**, 165311 (2022).
[50]I. Deriy, I. Toftul, M. Petrov, and A. Bogdanov, Phys. Rev. Lett. **128**, 084301 (2022).
[51]E. K. P. Chong and S. H. Żak, *An Introduction to Optimization* (Wiley, Chichester, England, UK, 2013).
[52]GitHub, see https://github.com/NikUstimenko/acoustotreams.git for "the acoustotreams code to simulate acoustic scattering based on the T-matrix method" (2025).
[53]D. Beutel, I. Fernandez-Corbaton, and C. Rockstuhl, Comput. Phys. Commun. **297**, 109076 (2024).
[54]COMSOL, see https://www.comsol.com/acoustics-module for "the pressure acoustics module in COMSOL Multiphysics" (2025).
[55]A. V. Kildishev, K. Achouri, and D. Smirnova, Adv. Opt. Mater. **13**, 2402787 (2024).
[56]B. Peterson and S. Ström, J. Acoust. Soc. Am. **57**, 2 (1975).
[57]M. Kafesaki and E. N. Economou, Phys. Rev. B **60**, 11993 (1999).
[58]I. E. Psarobas, N. Stefanou, and A. Modinos, Phys. Rev. B **62**, 278 (2000).
[59]R. N. S. Suryadharma, M. Fruhnert, I. Fernandez-Corbaton, and C. Rockstuhl, Phys. Rev. B **96**, 045406 (2017).